Chapter 5: DC Electric field-assisted formation of percolated silver nanolayers inside glass: Observations

5.1.1 Introduction

In the previous chapters it was shown that how a combination of a DC electric field and moderately elevated temperatures to a silver-doped nanocomposite glass could lead to dissolution of the silver nanoparticles in the glass matrix. From a macroscopic point of view, this effect was called "electric field-assisted dissolution" (EFAD). The phenomenon was physically interpreted in terms of ionization of the metal nanoclusters followed by the removal of ions from the clusters and their drift in the depth of the glass substrate.

Here, by using the EFAD technique, it is shown that how the conditions can be selected for which a buried layer of percolated silver clusters is formed several hundred nanometers below the glass surface, giving rise to almost arbitrary colours observable in reflection due to light interference. More generally, it is discussed how this technique could allow engineering of the optical properties of the material via gaining control over the spatial distribution of silver in the glass.

5.1.2 Experimental

For the experiments described in this chapter polydisperse type I-original samples (see chapter 3) were used. The electric-field assisted dissolution of Ag nanoparticles, as described in detail in chapter 4, was done by pressing two electrodes (7mm×9mm size) on the sample surfaces, the anode facing the layer containing nanoparticles. Then the sample was heated to a temperature of ~250°C, and a DC voltage was applied. For the main results presented here, once again the voltage was increased in steps of 0.2 kV to a maximum value of 1 kV within a total time of 50 min, keeping the current below 200 μA at any time; finally the voltage was disconnected and the temperature was reduced down to the ambient temperature.

5.1.2 Results and synopsis of observations

As it was described earlier the experimental procedure explained in the previous section leads to nearly complete bleaching of the area under the anode. As an example, Fig. 5.1 gives microscopic pictures of a bleached sample; the two pictures, presenting exactly the same sample area (where a corner of the anode was placed), were recorded in reflection (Fig. 5a) and transmission mode (Fig. 5b) of the

microscope (see the figure caption), respectively. In reflection mode the border region shows a rainbow-like pattern consisting of a sequence of several blue, green and red rings. In transmission mode (Fig. 5b), following the same path from untreated (location O) to treated area (location 6) of the sample, no rainbow pattern is observed, but only a gradual change of color from dark brown to faint yellow. The latter colors can be understood by the SP absorption of the silver nanoparticles being present in the sample initially, and their destruction by the dissolution process, governed by the strength of the electric field which quite obviously decreases with increasing distance from the anode edge. The remaining light yellow color within the bleached area indicates that a small amount of silver nanoparticles remains non-dissolved in the depth of the sample where the filling factor of nanoparticles is very low. This incomplete bleaching, as already observed and discussed, is due to the limited applied voltage of 1 kV. An important point here to note is that the bleaching extends slightly outside the electrode area (where the rainbow like pattern is observed).

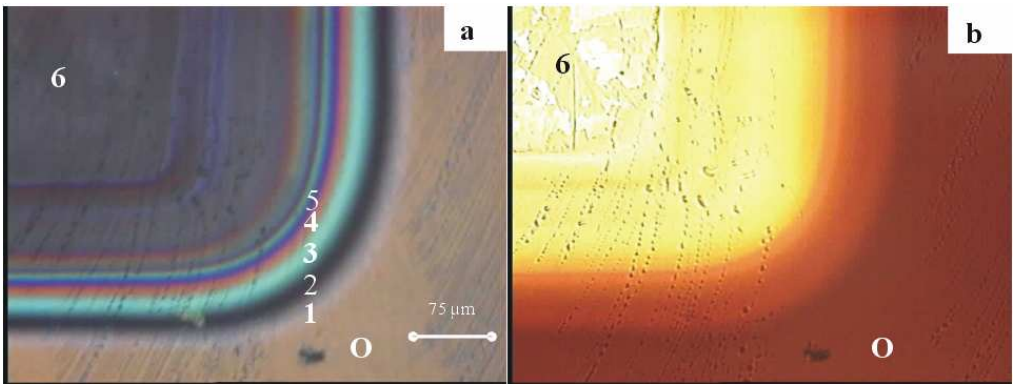

Figure 5.1: Photographs of the segment of the anodic surface of silver nanoparticles containing glass sample after treatment at 1kV, 250°C. Photographs were taken using a microscope spectrophotometer [MPM 800 D/UV, Zeiss] equipped with CCD camera in: (a) reflection and (b) transmission mode. Numbers (2-5) refer to locations where reflection spectra were measured (see Fig. 5.2).

To get an idea about the physical origin of the rainbow pattern, reflection spectra at different positions within the border region were recorded using a microscope spectrophotometer [MPM 800 D/UV, Zeiss], using a rectangular diaphragm of 1µm×10µm. The results are shown in Fig. 5.2, where the individual spectra are labeled along with the numbering of the locations as shown in Fig. 5.1a: at position 2 (in the first, dark blue ring) there is a rather high reflectivity of $R \approx 22\%$ at 380nm wavelength, but quite low reflectivity throughout most of the visible range; in contrast, the broad green ring (no. 3) exhibits a broad band of high reflectivity with a peak of $R \approx 24\%$ at 521 nm. The color of the next, red ring (no. 4) is obviously determined by the broad band of reflectivity around 633nm with $R_{max} \approx 23\%$, and finally the bright blue ring (no. 5) is characterized by the band around 459nm with maximum reflectivity of $R \approx 17\%$.

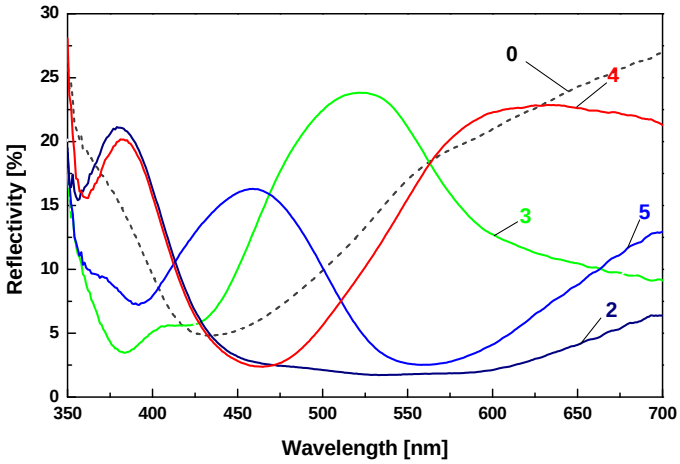

Figure 5.2: Reflection spectra measured at different locations on the sample surface using a microscope spectrophotometer [MPM 800 D/UV, Zeiss]. The reflection spectra are numbered according to different locations shown in fig. 6.1a. For more information refer to the text.

The most reasonable explanation for these spectra (and the whole rainbow pattern) is to assume that, during the dissolution process, an interface with considerable reflectivity in a variable depth of typically a few hundreds of nanometers has been produced and that the depth of the interface depends on the experimental conditions. At this rate the wavelength-dependent constructive or destructive interference between the light reflected at this layer and the light reflected at the sample surface would be the source of reflection spectra, and the different colors would be due to different depths of the interface.

In fact a very simple experiment was performed to check the plausibility of this assumption: if the colors are really due to interference, the rainbow pattern must change dramatically when the phase change by π upon reflection at the sample surface is cancelled by a highly refractive contact liquid dispersed on the sample surface. And in fact, a thin film of CH_2J_2 (n = 1.74) provided a dramatic change of the colors observed (Fig. 5.3), whereas a thin film of water (n = 1.33), not shown, did not change the pattern at all, only its brightness decreases considerably. The latter is compatible with the decreased reflectivity at the interface sample – liquid, as compared to the interface sample – air.

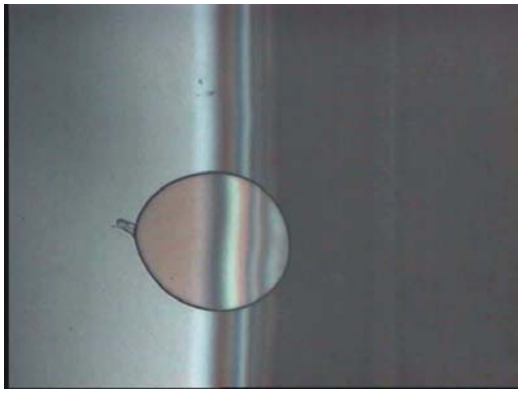

Figure 5.3: A photograph of segment of the sample with CH2J2 (n=1.74) on. During the experiment an area with small bubble was captured where a dramatic change of the observed pattern can be clearly seen.

While the idea of interference appears to be correct, the nature of the "interferometer" has to be clarified. In particular the following question has to be answered: which type of reflective layer is being produced during the electric field and heat treatment? For this purpose we studied the nanostructural changes in the samples using SEM. Fig. 5.4 shows the border region between modified (left-hand side) and unmodified (right-hand side) regions of a sample which was cleaved along a line crossing these regions; note the different length scales of top view (Fig. 5.4a) and side view (Fig. 5.4b). For both pictures the SEM signal refers to an electron penetration depth of ~ 100 nm, and silver particles appear as white spots.

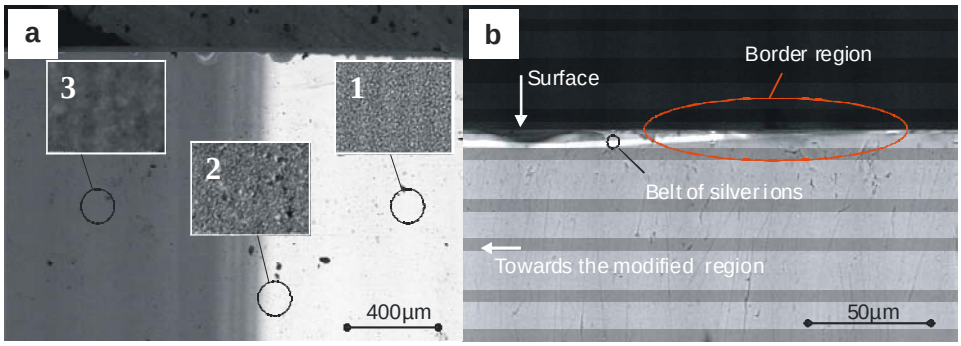

Figure 5.4: a) SEM picture of the surface of the sample taken in back scattered electron (BSE) regime (top view). Insets 1, 2 and 3 refer to locations in untreated region (location O in Fig. 5.1a), border region (location 1 in Fig. 5.1a) and modified region (location 6 in Fig. 5.1a), respectively. b) SEM picture of the cross section of the sample.

In the top view of Fig. 5.4a and the insets, which were taken at higher magnification, it is clearly seen that the originally very high concentration of silver nanoparticles close to the surface (inset-1) starts to decrease in the very border region (inset-2), until in the bleached area no remaining silver nanoparticles can be identified any more (inset-3).
The side view in Fig. 5.4b shows that in the treated area the nanoparticles were destroyed not only in the near surface region, but in the depth of the sample as well. Moreover, a shiny belt can be observed at a depth of approximately 5µm from the surface, the distance of this belt to the surface decreasing towards the border region. Silver ions, which were ejected from the nanopartcles during the dissolution process and drifted away in the depth, are at the origin of this belt, which could act as a buried reflective layer because of the depth gradient of ion concentration. In the second part of this chapter this aspect will be discussed in detail.

Fig. 5.5 gives the definitive proof of the interferential origin of the observed phenomenon and exhibits the nature of the buried reflective layer: in the central part of the microscope pictures of the original rainbow area (left, narrow part) and of the same region after the removal of a number of very thin surface layers by etching of the sample in 12% HF acid are shown. Clearly the rainbow pattern has changed dramatically due to the removal of surface layers. At the position indicated by white circles (green ring, location 3 in Fig. 5.1a) the sample was carefully examined by SEM before etching and after each etching step. At an etched depth of approximately

400nm a layer containing densely-packed percolated silver islands was observed (Fig. 5.5a).

Etching of a slightly deeper layer revealed that the silver filling factor is still very high in the depth (Fig. 5.5b). For comparison Fig. 5.5c shows the SEM picture taken from the very surface of the examined green region before etching, demonstrating again that the Ag particles close to the surface have been completely destroyed there. As it will be discussed later, this buried layer of densely-packed percolated silver clusters should, in principle, provide the reflectivity needed to observe, via interference, the rainbow colors in the border region.

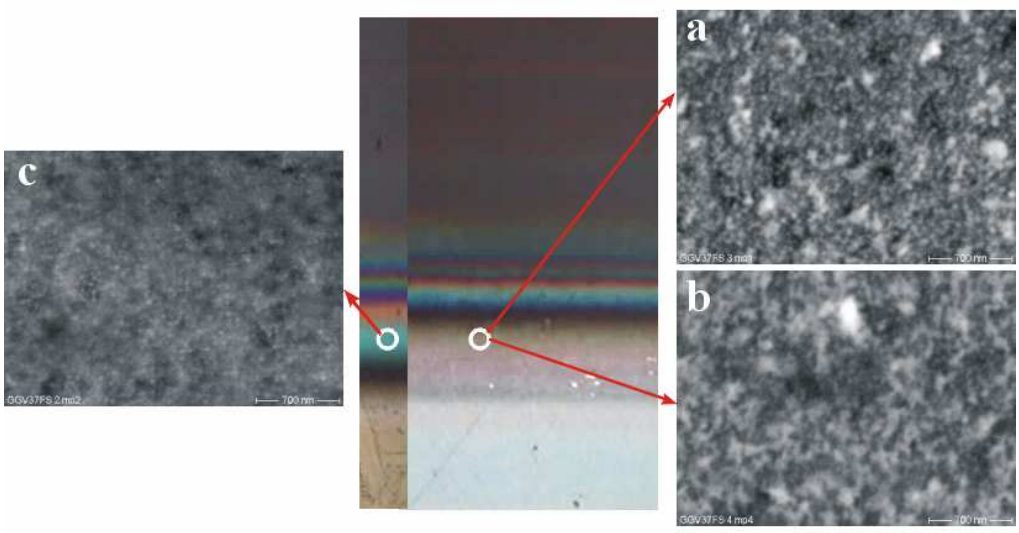

Figure 5.5: SEM pictures taken from the location of the first green ring (location 3 in fig. 5.1a). Pictures a and b were taken after successive etching of the sample surface up to depths of approximately 400nm. Picture c is presented for comparison and shows the surface of the sample before etching. The picture in the middle shows a segment of the border region of the sample before and after etching.

To the best of the author's knowledge, there is no closed description for the optical properties of percolated silver films up to now. Thus the brief discussion here is restricted to a plausibility check of the interface reflectivity. Generally speaking, percolated silver films represent an intermediate state between the limits (i) isolated nanoparticles and (ii) compact metallic film. The latter has, in case of silver, high reflectivity (R > 95%) throughout the visible range, caused by a very low refractive index (n ≈ 0.05) and strong absorption. Owing to the pertinent low penetration depth of typically 10 nm, silver films can be described by their bulk properties – e.g., maximum reflectivity – already for film thickness of ≈ 20 nm and above [5.6]. However, as it was described earlier (see chapter 2 and 3), the optical properties of isolated metal nanoparticles, representing the other limit, can often, up to quite high metal content, reasonably well be described using Maxwell-Garnett theory [5.1-5.4]. Based on this description, the complex refractive index of a composite medium with dielectric constant $\varepsilon_{eff}(\omega)$ can be expressed as:

$$n_{eff}(\omega) = \sqrt{\varepsilon_{eff}(\omega)}\,. \tag{5.1}$$

Using Eqs. (2.10), (3.3), (3.4) and the parameters $\varepsilon_h = 2.3$, $\omega_p = 9.2$ eV, $\gamma = 0.5$ eV, $\varepsilon_b = 4.2$, (see chapter 2 and 3), the optical constants $n(\omega)$, $k(\omega)$ of glass with spherical silver nanoparticles were calculated as a function of the volume filling factor of metal clusters in the glass matrix. Finally, Fresnel's formulae were applied to determine the reflectivity of an interface of the nanocomposite to the pure transparent matrix material (here glass with n = 1.5). The results of the calculation are shown in Fig. 5.6.

As it can easily be seen from Fig. 5.6, there is a strong dependence of reflectivity on the Ag filling factor, which influences both the real and imaginary parts of the effective refractive index of Maxwell-Garnett composite glass. At low filling factor ($f \leq 10^{-2}$) the reflectivity is negligible ($R_{max} \approx 10^{-3}$), while at quite high filling factor of $f \approx 0.3$ the required reflectivity $R \geq 20\%$ is achieved throughout the visible range. However at such high filling factors the Maxwell Garnett model is no longer a very accurate description of the optical properties, in particular not for the case of early-stage percolation as observed for the buried layers in this work. So it makes no real sense to try to simulate the observed interference spectra on the basis of this too simple model, although some qualitative agreement can be achieved assuming depths of 100 to 400 nm for the buried layer.

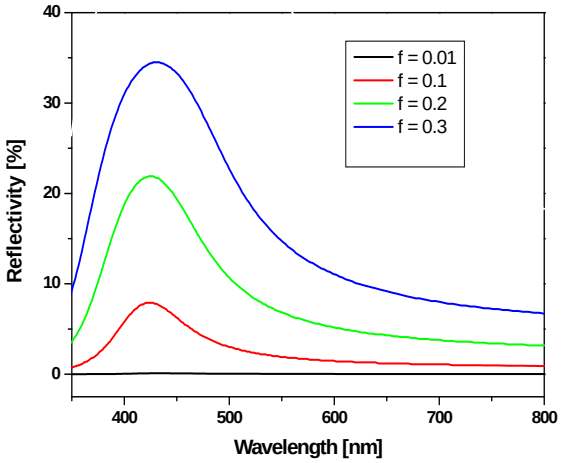

Figure 5.6: Calculated reflectivity for interface between Maxwell-Garnett silver in glass nanocomposite and neat glass, with fill factor *f* as parameter

On the other hand these simple considerations allow us to draw the important conclusion that already a rather thin layer of only a few tens of nanometers with relatively high silver content will definitely be able to provide the reflectivity needed to explain the reflection spectra observed by interference.

Based on the above observations the buried layer close to the border region is created due to the following mechanism: the combination of DC electric field and temperature at first induces destruction of silver nanoparticles at the upper layer close to the surface of the sample. Further treatment, i.e. increase of the applied voltage, results in the drift of silver cations in the depth of the sample, and simultaneously electrons are attracted towards the anode, in the opposite direction of the cation movement. So at some depth the electrons may neutralize the cations again, thereby increasing the silver concentration there, which can lead to percolation and production of a layer containing densely-packed percolated silver clusters. The threshold of the dissolution process depends strongly on the filling factor of the nanoclusters (See chapter 4).

Thus, the magnitude of the voltage applied to a sample with a gradient of the nanoparticle filling factor defines the distance between the surface and the buried layer of percolated silver clusters. This layer, finally, acquires a reflectivity that is high enough to observe interference of light reflected at the sample surface and at the buried layer. Since, in the border region the applied electric field – and thus the depth of this reflective layer – is non-uniform, rainbow-like patterns can be observed there.

At this point the obvious question occurs whether similar experiments are possible, in which the experimental parameters such as electric field, temperature and processing time are chosen so that a larger homogeneous area of interference is produced, and hence a uniformly colored region. For this purpose some preliminary experiments were conducted, where DC voltages of 200 V, 400 V, and 600 V were applied at ~250°C in one step, for a total time of 30 min; electrodes with an area of 1 mm×2 mm were used. Due to imperfect contact (See chapter 4) not the whole regions under the electrodes were homogeneously colored, but at least areas with dimensions of several 100 µm were produced which appear predominately in blue, green and red. In Fig. 5.7 two pictures show the edges of the green and red regions produced.

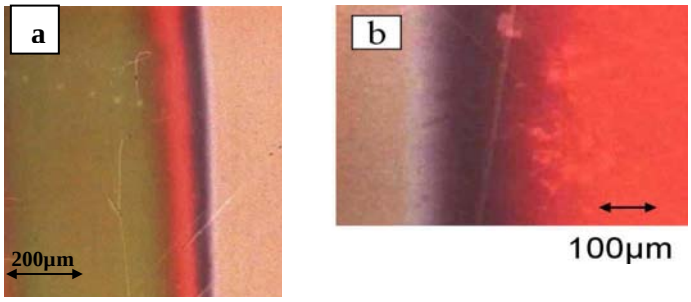

Figure 5.7: Preliminary results showing large-area coloration through electric-field-assisted production of a buried percolated silver layer; processing at **(a)** 400V and **(b)** 600V.

For further analysis a sample which was exhibited large green area (Fig. 5.7a) was cleaved and its cross section was then subjected to SEM examination. Fig. 5.8a shows the results. The buried layer responsible for the green colour in this sample can be identified. The distance between this layer and surface of the sample was estimated from the SEM to be ~500nm. For comparison Fig. 5.8b shows the cross section of untreated (original) region of the sample (polydisperse type I-original).

Once again it can be clearly seen that the described treatment results in dissolution of silver nanoparticles starting from the very surface of the sample and down to a particular depth (here ~480nm) depending on the magnitude of the applied voltage.

The last remark which has to be pointed out is that the size of the produced monochromatic area in each case was only limited by the size of the electrodes used providing that there is a good contact between the sample and anode. This obviously requires good quality of both surface of the sample and the electrodes used. This requirement is in fact put an upper limit on scalability of the described technique.

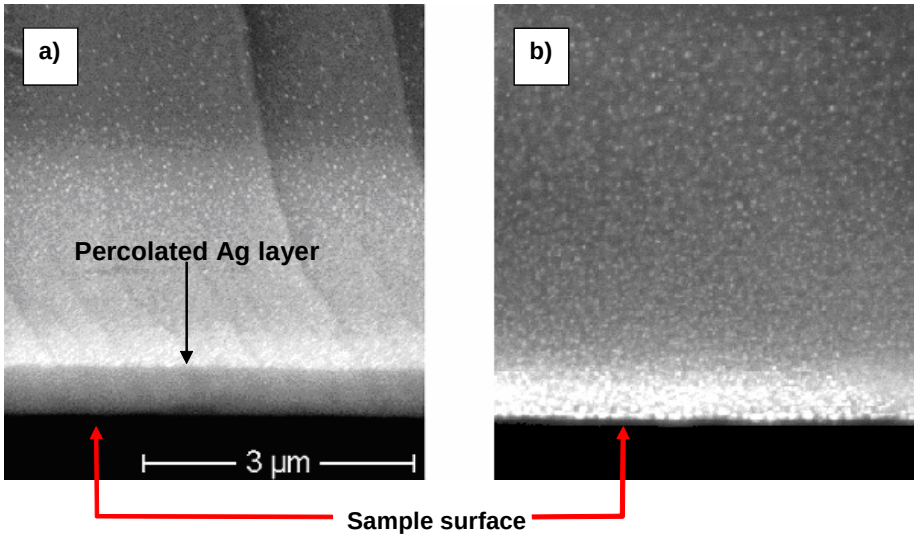

Figure 5.8: a) SEM picture taken from the cross section of the sample exhibiting large green area. **b)** Shows the cross section of the original (untreated) area of the same sample.

Now that the main experimental achievements were presented and a synopsis of the results was given, it is the time to introduce a more accurate model for description of the interference spectra.

5.2 DC Electric field-assisted formation of percolated silver nanolayers inside glass: Characterizations

5.2.1 Introduction

Here, following the results presented in the previous part, the optical characterization of silver-doped glasses subjected to electric field-assisted dissolution of nanoparticles is presented. The characterization is performed by means of fitting of the spectrophotometric measurements.* The optical properties of the investigated samples are described in terms of the interference between the light reflected from the glass surface and the light reflected from a silver-containing layer formed in the depths of the glass.

The analysis of the data reveals the porosity of the glass in the region where nanoparticles are dissolved, that can be attributed to the presence of residual nanopores. The procedure starts by employing a simple model to represent the physical structure of the samples. The complexity of the model then increases until a satisfactory description of the experimental data is achieved. This approach allows determining the critical parameters that control the optical properties of the buried silver-containing layer as well as the glass region where the nanoparticles are dissolved.

5.2.1 Model

As it was said earlier, due to the changes in the structural properties of the samples, the coloration observed in reflection can be easily understood in terms of interference between the light reflected from the glass surface and the light reflected from the buried silver-containing layer. Depending on the intensity of the applied electric field, this layer will be formed at different depths, changing the interference condition of maxima and minima and giving place to a different coloration. Thus, in the border region, due to the gradient of the electric field intensity, there will be a depth-gradient of the silver-containing layer, originating a continuous variation of the coloration (rainbow-like pattern). Partial bleaching of the sample, as was discussed earlier, can be attributed to the fading of the associated surface plasmon absorption due to the dissolution of nanoparticles. The aim at this point is to find a physical model for the treated regions that can explain the observed coloration. The reliability of the model will be checked by fitting the measured reflectance spectra, since the

* Fitting of the experimentally measures spectra were performed by Dr. Sancho-Parramon using NKDSoftware [5.7].

measured transmission is very low due to the surface plasmon absorption of the remaining nanoparticles and hence does not provide significant quantitative information.

In order to simulate the measured reflectance spectra, it is necessary to determine the reflectivity of the buried silver-containing layer and therefore it is indispensable to establish an appropriate model for the description of its optical constants. A widely exercised approach for modelling the optical properties of composite media is via the effective medium theories, namely Maxwell-Garnett theory (MGT) and Bruggeman effective medium approximation (BEMA). Since the optical behaviour observed in the reflectance spectra is dominated by interferential effects, in order to reproduce the experimental data it is necessary to use calculations for the propagation of light in stratified media.

For the calculations general-purpose software for the optical characterization of multilayer stacks, namely NKDSoftware [5.7], is used. This software allows defining a multilayer structure where each layer is described by few parameters: typically, its thickness and a variable number of parameters accounting for the dispersion of the optical constants of the layer material. In this way, the optical behaviour of the sample is completely represented with a set of parameters, whose optimal value can be found by the minimisation of the ξ^2 merit function defined as:

$$\xi^2\left(P_1, P_2, \ldots, P_{N_p}\right) = \frac{1}{n_{meas} - N_p - 1} \sum_{i=1}^{n_{meas}} \left[\frac{y_i - y\left(x_i; P_1, P_2, \ldots, P_{N_p}\right)}{\sigma_i} \right]^2 , \qquad (5.2)$$

where n_{meas} is the number of measured points, y_i are the experimental data measured at the wavelength x_i, and σ_i are the associated experimental measurement errors. P_1, P_2,…P_{Np} are the N_p parameters defining the sample and $y(x_i,\ldots,P_1, P_2, \ldots, P_{Np})$ are the data calculated with standard algorithms for computing the optical properties of multilayer structures [5.8, 5.9].

The software presents some particular features, as the possibility to use different effective medium approximations for representing layers made up of mixtures of materials. It also allows accounting for in-depth inhomogeneity of the refractive index within the layers, assuming different mathematical profiles for the variation of the refractive index through the layer thickness.

5.2.2 Characterization of the large coloured areas

In this Section the results of modelling of the optical properties of the regions were the electrodes were placed are presented. The attention is focused on a sample where the green colour in reflection was observed (Fig. 5.7a). As previously mentioned, the SEM cross view of the treated area (Fig. 5.8a) evidenced dissolution of the silver nanoparticles in a region of approximately 500 nm and formation of a thin buried silver-containing layer at this depth. The presence of none-dissolved nanoparticles at deeper regions of the glass can also be observed.

According to the SEM picture, the simplest multilayer model that could describe the optical behaviour of the sample would be a 2-layer structure: a glass surface layer where nanoparticles were dissolved and the buried silver-containing layer. The rest

of the glass would only play the role of substrate, thick enough to neglect interferential effects. Fig. 5.9 shows a schematic diagram of the model.

In order to describe the glass surface layer and the glass substrate, their optical constants are fixed to those found in literature for soda-lime glass. At this stage the effect of the none-dissolved nanoparticles in the glass substrate are neglected due to the very low filling factor. It was assumed that the buried silver-containing layer is a mixture of glass and silver (with optical constants for the silver taken from the literature [5.10]) and its optical constants is modelled using the effective medium theories. Thus, the first model requires a total of 3 parameters: the thickness of the glass surface layer (d_{glass}), the thickness of the buried silver-containing layer ($d_{Ag\text{-}glass}$) and the filling factor of silver in the buried silver-containing layer (f_{Ag}).

If the MGT is used to represent the optical properties of the buried silver containing layer, the achieved fitting of the data reaches a value of the merit function of ξ^2=16.8, with the following values of the optimized parameters: d_{glass} = 546 nm, $d_{Ag\text{-}glass}$ = 83 nm and f_{Ag} = 0.05. However, if the BEMA is used, a significantly better fitting is obtained (ξ^2=5.4) with the parameter values d_{glass} = 547 nm, $d_{Ag\text{-}glass}$ = 29 nm and f_{Ag} = 0.14. Figure 5.10 contains the fit achieved using the BEMA for the buried silver-containing layer (See red line).

A simple observation of the simulation obtained with the previous modelling reveals that the discrepancies between the computation and the experimental data are mainly found in the values of the maxima and minima of the spectra, while the position of the fringes is well tuned. Typically, such discrepancies are related to an in-depth inhomogeneity of the refractive index of the layers [5.11]. In chapter 4 a plausible explanation proposed which could describe such inhomogeneity, plain-view SEM pictures of the modified area suggested the presence of hole-like structures in the region where nanoparticles were dissolved (Fig. 4.5).

In this way, this region may have a notable porosity that would lower the refractive index of the glass. However, since the pores would be originated by the dissolution of nanoparticles and nanoparticles were embedded at a distance of a few tens of nanometer from the glass surface, the very surface of the glass would be compact. In this case, a more realistic model for the sample would be represented by a 3-layer structure on a glass substrate: a very thin layer of compact glass, a porous glass layer (where the nanoparticles were embedded in the initial sample), and the buried silver-containing layer. Fig. 5.11 shows a schematic diagram of the model.

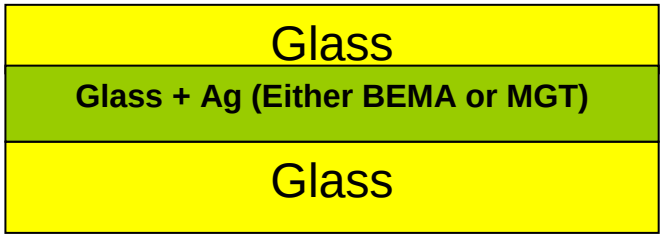

Figure 5.9: Schematic diagram of the 2-layer model.

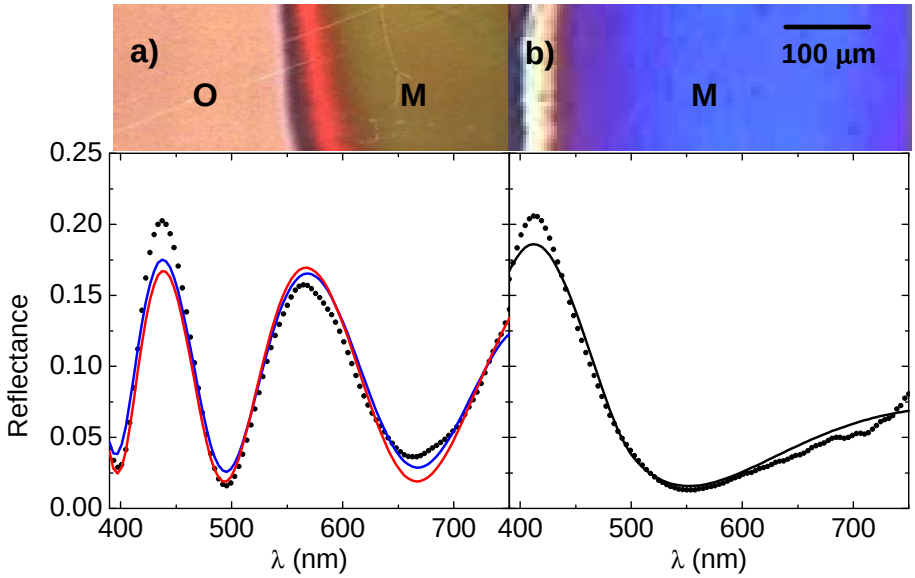

Figure 5.10: a) Measured reflectance spectra of the area showing a green coloration (dots) together with the fits assuming: i) a 2-layer model (Fig. 5.9): glass layer and BEMA silver-containing glass layer (red line) and ii) a 3-layer model (Fig. 5.11): glass layer, homogeneous porous glass layer and BEMA silver containing layer (blue solid line). **b)** Measured reflectance spectra of the area showing a blue coloration (dots) together with the fit assuming a 3-layer model: glass layer, inhomogeneous porous glass layer with a pore concentration equal to the original distribution of silver nanoparticles and BEMA silver containing layer (solid line).

The optical constants of the porous layer can be represented using effective medium approaches, considering a mixture of glass and voids. Furthermore, we shall primarily assume that the concentration of pores will be the same as the concentration of silver nanoparticles in the untreated sample. As far as the silver filling factor near the surface varies approximately as (see Fig. 3.1b):

$$f(x) = 0.7 - 0.6x \ , \tag{5.3}$$

where x is the glass depth in microns.

The thickness-dependence of the refractive-index of this layer is implemented dividing the layer in a fixed number of sub-layers of equal thickness. Each sub-layer is modelled with the BEMA, with a pore concentration calculated according Eq. 5.3. Now the model of the sample requires 4 parameters: the thicknesses of the 3 considered layers (d_{glass}, $d_{porous\text{-}glass}$, $d_{Ag\text{-}glass}$) and the filling factor of silver in the buried layer (f_{Ag}). This model enables a significant improvement of the description of the data, as the merit function reduces to 3.92. The values of the optimized parameters are: d_{glass}=30 nm, $d_{porous\text{-}glass}$=619 nm, $d_{Ag\text{-}glass}$=28 nm and f_{Ag} = 0.1. Similar results are achieved if the MGT is employed. This is due to the fact that glass and voids both have relatively similar optical constants (specially, compared to the difference between the optical constants of silver and glass) both theories lead to similar results [5.12].

Even though a significant improvement in the description of the data was obtained, our primer assumption that the porosity in the treated sample exactly follows the filling factor distribution of silver nanoparticles in the untreated sample may be rough; as it neglects the possible collapse of the pores once the silver is dissolved.

In this sense, it seems necessary to check if another value of the pore concentration can lead to a significantly better data fitting. For this reason, we shall now consider the pore concentration as another parameter which has to be optimized. In order to avoid an excessive number of parameters, a constant homogeneous concentration of pores through the layer where nanoparticles are dissolved, is assumed. This parameter is defined by the pore concentration f_{pores}.

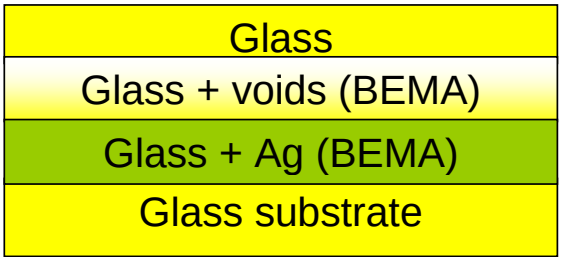

Figure 5.11: Schematic diagram of the 3-layer model.

Therefore, a total of 5 parameters will define the sample (d_{glass}, $d_{porous\text{-}glass}$, $d_{Ag\text{-}glass}$, f_{Ag}, f_{pores}). Using this modelling, a slight improvement of the data is reached ($\xi 2$= 3.2), with the parameter values: d_{glass} = 39 nm, $d_{porous\text{-}glass}$ = 570 nm, d_{Ag}=23, f_{Ag} = 0.1, f_{pores} = 0.29. This concentration of pores is lower than the average concentration of silver in the original sample in the same thickness (~0.5). The fitting of the data using this model is shown in Fig. 5.10a by blue line.

In order to assess the validity of the model, it was also applied to the sample where a blue coloration was observed via application of 0.2kV). Once more it was assumed that the pore concentration follows the original distribution of silver nanoparticles. A good fitting of the data is obtained, with a value of the merit function of 1.3. The value of the optimized parameters is d_{glass} = 39 nm, $d_{porous\text{-}glass}$ = 279 nm, $d_{Ag\text{-}glass}$= 19 nm and f_{Ag} = 0.02.

Fig. 5.10b shows the reflectance spectra for this sample, evidencing the good agreement between the simulation and the experimental data. Similarly to the analysis of the green coloured sample, it was also checked if another value of the pore concentration could lead to a better fitting of the data. With the pore concentration as a free parameter, the merit function decreases only to 1.29, with the parameter values d_{glass}=42 nm, $d_{porous\text{-}glass}$=272 nm, d_{Ag} =17 nm, f_{Ag}= 0.01, f_{pores}=0.67. In this case, the pore concentration is closer to the average filling factor of silver in the original sample in the same thickness (~0.6).

A summary to what was said so far would contain the assessment on the initial qualitative explanation for the observed coloration of the treated samples: the interference between the light reflected at the glass surface and the light reflected in a thin layer containing silver. Such layer can be well modelled as a mixture of glass and silver within the BEMA, rather than with the MGT. Furthermore, the refinement of the data fitting reveals the presence of pores that was already suggested by previous SEM observations which seems to be originated via the dissolution processes

5.2.3 Characterization of the border region

Here the aim is to extend the obtained model to the border region of the sample where the rainbow-like pattern was observed. It is done due to the fact that the phenomenon has the same physical origin. The reflection spectra presented in Fig. 5.2 were fitted using the model consisting of 3 layers (compact glass layer, porous glass layer, silver containing layer). It is assumed that the porous layer is homogeneous, and the pore concentration as a parameter which has to be optimized. Furthermore, it is impose that the compact glass layer will have the same thickness for the fitting of all the spectra, allowing a reduction of the total number of necessary parameters.

The results of the data fitting using this modelling are summarised in Table 5.1. While the description of the light blue and red spectra is quite good, the fits for the green and dark blue spectra are rather unsatisfactory, as indicated by the obtained values of the merit function. The fittings of these locations become even worse if in order to simulate the distribution of pores in the rainbow area the original distribution of silver is considered.

The most suitable explanation for the failure of the model in describing of the two last spectra is that they are taken in the regions very close to the untreated area. Therefore, one can expect that the effective DC electric field is significantly lower than under the electrodes area and that the depth of the buried silver-containing layer should be smaller. In this case, there might be a strong influence of the none-dissolved nanoparticles, situated beneath the buried layer and in the depth of the glass.

Spectra	d_{glass} (nm)	$d_{porous\text{-}glass}$ (nm)	f_{pores}	$d_{Ag\text{-}glass}$ (nm)	f_{Ag}	ξ^2
Light blue (4)	44	238	0.1	27	0.11	1.17
Red (3)		198	0.54	34	0.09	0.97
Green (2)		137	0.46	60	0.04	6.80
Dark blue (1)		25	0	35	0.2	3.4

Table 5.1: Value of the optimised parameters resulting from the reflectance fitting of the different locations of the border region area using a 3-layer model (glass layer, porous glass layer, BEMA silver containing layer).

In fact, the SEM pictures of the border region of the sample have already revealed the presence of none-dissolved nanoparticles (See Fig. 5.4a). To account for these remaining nanoparticles, it is assumed that beneath the buried layer there is a gradient of silver nanoparticles, with a filling factor that decreases linearly from a maximum value f_L to zero within a certain thickness $d_{Ag\text{-}nano}$:

$$f(x) = -\frac{f_L}{d_{Ag-nano}} x + f_L . \tag{5.4}$$

According to the initial distribution of the nanoparticles, an exponential variation of the silver filling factor would be more appropriate; however the linear model is simpler and would allow us to check easily the role of the remaining none-dissolved nanoparticles.

Thus, the model for the border region will consist now on a 4-layer structure: the surface glass layer, the porous glass layer, the buried silver-containing layer and the layer with a linear filling-factor gradient of remaining none-dissolved nanoparticles. A schematic diagram of this model is presented in Fig. 5.12.

The gradient of this layer is implemented by dividing the layer in a fixed number of sub-layers of equal thickness and calculating the filling factor of silver nanoparticles for each sub-layer according to Eq. 5.4. However, now the effective optical constants of the sub-layers are calculated using the MGT, since it is more appropriate for the topology of none-dissolved nanoparticles. In this model two more parameters which both have to be optimised are introduced: the thickness of the layer containing none-dissolved nanoparticles ($d_{Ag\text{-}nano}$) and its maximum filling factor (f_L).

With this model, the fittings of the green and dark blue spectra are significantly improved, as listed in Table 5.2, together with the value of the optimized parameters. The fits of the spectra of the rainbow-like region are shown in Fig. 5.13. It has to be pointed out that the remaining none-dissolved nanoparticles do not have significant weight neither in the other spectra of the border region or in the coloration of the treated areas.

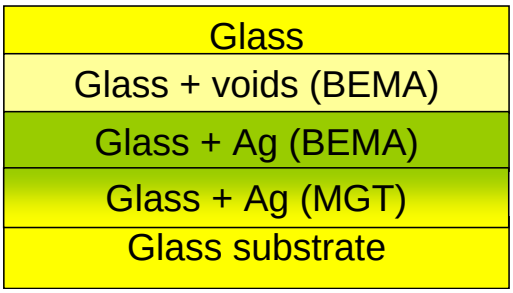

Figure 5.12: A schematic representation of the 4-layer model.

Spectra	d_{glass} (nm)	$d_{porous\text{-}glass}$ (nm)	f_{pores}	$d_{Ag\text{-}glass}$ (nm)	f_{Ag}	$d_{Ag\text{-}nano}$ (nm)	f_L	ξ^2
Light blue (4)	45	242	0.12	25	0.10	-	$<10^{-5}$	1.15
Red (3)		191	0.48	38	0.08	-	$<10^{-5}$	0.96
Green (2)		124	0.53	41	0.02	768	0.09	0.80
Dark blue (1)		14	0.78	0	0	690	0.12	1.85

Table 5.2: Value of the optimised parameters resulting from the reflectance fitting of the different locations of the border region using a 4-layer model (glass layer, porous glass layer, BEMA silver containing layer and inhomogeneous MGT layer with silver nanoparticles).

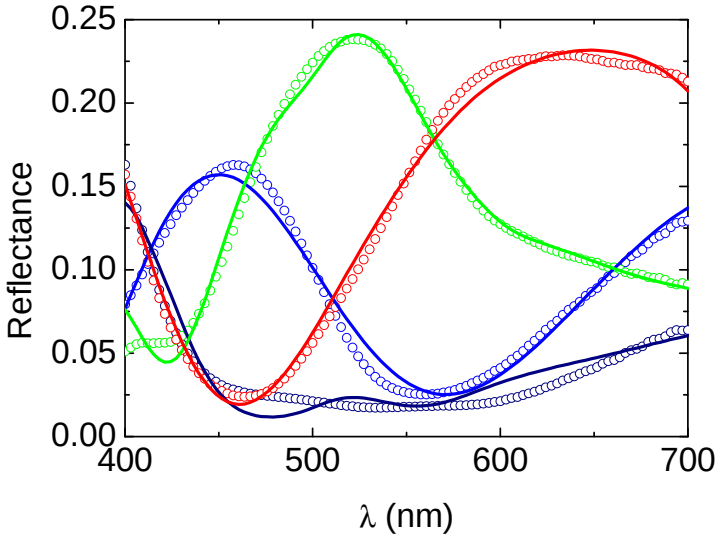

Figure 5.13: Measured reflectance spectra of the different locations of the border region (dots) together with the fits assuming a 4-layer model: glass layer, homogeneous porous glass layer, BEMA silver containing layer and inhomogeneous MGT layer with silver nanoparticles (solid line). The different locations in the Figure are indicated by different colors.

5.3 Discussion

The use of interferential calculations for the description of the experimental measurements is very satisfactory, assessing the qualitative explanations proposed earlier to describe the modification of the optical properties of the samples. Thus, the buried silver-containing layer seems to be responsible for the observed phenomenon. It is found that the buried silver-containing layer is better described within the frame of the BEMA than the MGT. It was assumed that such layer is formed by the aggregation of silver ions in heterogeneous clusters from the dissolved silver nanoparticles, with a possible interconnection among clusters (percolation), and hence the picture agrees better with the BEMA assumptions than with the MGT. From a numerical point of view, the BEMA provides the buried layer with a rather high absorption (and thus, reflectivity) through the whole visible spectral range (as we observe experimentally), while the MGT can only give a significant reflectivity in a narrow region around the surface plasmon resonance (centred approximately at 400 nm). The comparison between the MGT and BEMA is only shown for the simplest model (the 2-layer model consisting of a compact glass layer and the buried silver containing layer), but as it was checked for all the other tested models the BEMA gives significantly better fittings than the MGT, with merit functions approximately 3 times smaller.

The depth of the buried silver-containing layer resulting from the fittings (given by the sum of the parameters d_{glass} and $d_{porous\text{-}glass}$) is in a fair agreement with the values determined by SEM for the sample exhibiting green coloration (~500 nm, with a resolution of several tens of nanometers). The depth of this layer for the sample exhibiting blue coloration is smaller; around 300 nm what can be expected due to the applied DC voltage was lower for this sample. The thickness of the buried layer can not be well estimated from the SEM pictures, indicating that it should have a value around a few tens of nanometers, what agrees with the obtained values for all the

tested models. The thickness and the silver concentration of the buried layer is lower for the blue coloured sample than for the green one, as can be expected from the experimental conditions: the lower the applied voltage, the lower the total amount of silver that will be dissolved and form part of the buried layer.

In any case, the filling factor of silver in this layer seems to be low if compared with the high concentration of silver that is suggested by the SEM images. The values found by the data fitting refer exclusively to metallic silver (i.e: silver with a "metallic" optical behaviour). The dissolution of nanoparticles is produced via the ionization of silver and therefore the silver that is present in the buried layer could be mainly in the form of cations, undistinguishable from metallic silver by SEM. Silver cations do not play an important role in the optical properties of glass in the visible spectral range [5.13]. Hence, it can be assumed that the presence of the silver ions do not substantially modify the optical constants of the glass, especially if compared with the effect of metallic silver.

In fact, the required concentration of silver which has to be achieved in order to observe the reflectance can be roughly estimated from the following expression [5.14]:

$$R = \frac{R_1 + R_2 + 2\sqrt{R_1 R_2}}{1 + R_1 R_2 + 2\sqrt{R_1 R_2}}. \qquad (5.5)$$

This equation relates the maximum reflectivity (R) of a single dielectric layer on an absorbing (metallic) substrate, being R_1 and R_2 the reflectivity of the air-dielectric and dielectric-metal interfaces, respectively. Thus, assuming a refractive index of 1.5 for the glass, in order to obtain a value of R = 20% (maximum values observed in the experimental spectra), a value of R_2 ~10% is required. This value can be achieved in the visible spectral range with a silver filling factor of ~10% using the effective medium theories. Since the refractive index of the glass is actually lower due to the porosity, the filling factor of silver can be even lower to reach the same value of R.

The refinement of the data fitting reveals that the glass beneath the surface should have a lower refractive index that can be explained by the presence of nanopores originated by the dissolution of silver nanoparticles. The assumption that the distribution of pores follows the filling factor distribution of silver nanoparticles in the original sample enabled us to achieve a fairly good description of the data. By considering a different pore concentration only led to a slightly better fitting for measurements of the green coloured sample. This particular result suggests a lower pore concentration. This could be understood in terms of a partial collapsing of pores. This phenomenon may depend on the treatment conditions, since no improvement was achieved in the case of the blue coloured sample. More complex mathematical models for the distribution of pores were also tested; however, they only led either to the same results or to physically meaningless results. In any case, the confirmation of the presence and distribution of pores will be the subject of future research.

The extension of the model to the description of the optical behaviour of the border region is partially satisfactory. While the spectra of the border region closer to the treated area can be successfully fitted, the model scarcely describes the spectra

measured in locations close to the untreated area. However, if the contribution of the remaining none-dissolved nanoparticles is taken into account (through a linear gradient of filling factor of nanoparticles in the depth of the glass), the measured spectra can be remarkably reproduced. It has to be pointed out that the contribution of the gradient of none-dissolved nanoparticles was not able to improve the fitting of the light blue and red spectra of the border regions. Actually, looking at the value of the parameters, on can observe that the gradient starts at a maximum value of 12% of Ag nanoparticles for the dark blue spectra and at 9% for the green one. Therefore, we can expect that it would have even lower values for the spectra of the border region taken closer to the treated area and, consequently, a very weak weight in the reflectance spectra.

From the value of the optimised parameters (Tab. 5.2), it can be established that the depth of the buried silver-containing layer diminishes as the spectra correspond to locations approaching to the untreated area. This result can be expected from the lowering of intensity of the DC electric field in the border region. The concentration of pores also increases in the same direction, suggesting that the pores are inhomogeneously distributed and mainly concentrated in a region very close to the surface, as expected from the distribution of silver in the original sample. Nevertheless, the considered value for the pore concentration is lower than the average filling factor of silver in the original sample, once again indicating the possibility of a partial collapse of pores after the dissolution of silver. The total amount of silver in the buried layer (estimated by the product of layer thickness and silver concentration) decreases for the spectra closer to the untreated area. This behaviour suggests that the buried silver layer can be hardly defined for the locations close to the untreated area. In fact, for the dark blue spectra, the presence of this layer is overlooked by the optimisation procedure. Therefore, the interference effects in the border region closer to the untreated area seem to be originated by the remaining none-dissolved nanoparticles, rather than by the buried silver-containing layer.

A typical problem in the optical characterization of materials is the use of a large number of parameters that can lead to numerically good solutions but lacking of physical sense. Here the procedure started with a very simple model and test more complex models in successive steps, according to the information provided by the structural characterization of the sample. The improvement in the modelling is evaluated by the reduction of the values of the merit function. In this way, the possible use of an excessive number of parameters that do not allow a noteworthy improvement in the description of the experimental data was avoided.

5.4 Summary

In the first part of this chapter by applying an intense DC electric field at $\leq 250°C$ to a glass containing silver nanoparticles in a thin surface layer of a few microns, a buried layer of percolated silver clusters with modified optical properties was produced. The buried layer was located in the border region between the treated and untreated regions of the sample. Reflection of light from the buried layer and its interference with the light reflected from the surface of the glass is thought to be responsible for the observed rainbow-like pattern.

Scaling of this technique via varying the applied voltage resulted in production of large areas which show homogeneous colors in reflection. In each case the distance between the produced buried layer and the surface of the sample was strongly dependent on the magnitude of the voltage applied. Once again reflection of light from the buried layer and its interference with the light reflected from the surface of the glass is believed to be responsible for the observed spectra in each case.

In the second part fitting of the measured spectra revealed that the observed optical behaviour can indeed be successfully explained in terms of interferential calculations. Furthermore, the fitting procedure allows establishing what parameters determine the coloration. Thus, the buried layer seems to have a thickness of a few tens of nanometers, with a 10% content of metallic silver that can be well described within the BEMA. The fitting of the data also suggests the presence of pores beneath the glass surface that can be formed by the dissolution of silver nanoparticles. The coloration observed in the border region can also be explained with this model, although the interferences for the spectra measured in locations closer to the untreated area originate from the light reflected by the region with none-dissolved nanoparticles in the depth of the glass.

Further thorough studies of the threshold and intermediate conditions as well as dynamics of the process are needed; this will be a subject of future work. What is clear, however, is the potential offered by this simple technique to produce, based on metal-doped nanocomposite glasses, devices with a need for wavelength selection.